



Chromium doped ZnO nanoparticles for energy storage, gas and humidity sensing and spin based electronic devices applications

N. M. Moussa¹ · F. M. Ebrahim¹ · K. Adly² · M. Y. Hassaan¹

Received: 22 April 2022 / Accepted: 2 August 2022 / Published online: 13 September 2022
© The Author(s) 2022

Abstract

This work was suggested to study the impact of Cr ions doping on the structural, optical, electrical and magnetic behavior of ZnO nanoparticles (NPs). The $Zn_{1-x}Cr_xO$ (with $0 \leq x \leq 0.14$ wt %) samples were fabricated by the co-precipitation technique. The obtained samples were characterized by the X-ray diffraction (XRD) technique, (FTIR) spectroscopy, UV–vis spectrophotometer, Ac measurements and Vibrating Sample Magnetometer (VSM). As a key results of all the mentioned above tools we can be summarized them as following; XRD patterns showed the presence of wurtzite (hexagonal) crystal structure with secondary phase formation in all doped samples. Also, it was found that as Cr ions were increased the particle size showed gradually decreasing in the samples that doped with Cr ions content of (0.06 and 0.1 wt %), while at 0.14 Cr content a slight increase was observed. The FTIR spectroscopy spectra showed the existence of chromium ions in the structure of ZnO nanoparticles. UV–vis spectra showed a red shift in the centers of the absorption bands. The energy band gap was found to be increased from 3.84 to 4.02 eV with increasing Cr content. The dielectric parameters such as, dielectric constant (ϵ') and dielectric loss ($\tan\delta$), were investigated as a function of frequency and Cr doping content. The results showed increasing values of ϵ' at lower frequencies especially with high Cr doping content, whereas $\tan\delta$ gives a higher value for the blank sample at a lower frequencies and decreased as the doping of Cr concentration increased. The ac conductivity (σ_{ac}) for Cr doping samples showed increasing values, especially the sample of 0.14 wt % Cr concentration. In addition, the Cr doped ZnO nanoparticles exhibited a ferromagnetic behavior at room temperature. All the results obtained from the different techniques were considered promising for different applications i.e. energy storage devices, gas and humidity sensing and spin based electronic devices applications.

Keywords Cr doped ZnO nanoparticles · Co-precipitation method · Optical properties · Electric properties · Ferromagnetism · High frequency operation · Charge storage · Gas and humidity sensing · Spin based electronic devise

✉ N. M. Moussa
xpnasser@yahoo.com

¹ Physics Department, Faculty of science, Al- Azhar University, Cairo, Egypt

² Physics Department, Faculty of Science, Suez Canal University, Ismailia, Egypt

1 Introduction

Nanostructure materials have shown superphysical features that differ from bulk materials over the previous few decades, although they are considered to be promising for the development of new electronics (Omri et al. 2016). It is also regarded that an extensive variety of nano-sized powders have been fabricated for different applications such as electrical and optical applications (Moazzen et al. 2013). Recently, II-VI semiconductors have been intensively studied for photonic and optoelectronic applications (Khan et al. 2018a; Arora et al. 2014). ZnO is a promising and extensively well-studied II-VI semiconductor with a straight band gap energy of 3.37 eV and a significant exciton binding energy of (60 meV). Nano-spheres, nano-rods, nano-powders, nano-flowers, and nano-wires are all examples of ZnO nano-structures. With size modulations, this nanostructure ZnO exhibits fascinating optical, dielectric, and other physical properties, positioning it as the most promising candidate for the production of nano-devices (Li et al. 2007).

Pure ZnO contains a wide range of inherent defects, including substitutional and interstitial Zn vacancies, paramagnetic O vacancies, and interstitial O. These inherent defects are typically produced in the band gap at the acceptor or donor stages, and they alter the physical properties of ZnO. Recent research has focused on its application in short-wavelength optoelectronic devices (Zargar et al. 2020), Zhigang Zang et al., have studied the effect of ZnO nanoparticles decoration on different types of perovskite thin films to be used as optoelectronic materials (Li et al. 2017; Wang et al. 2020). ZnO nanoparticles has many different applications such as photocatalytic, dentistry and solar cell (Pushpalatha et al. 2022; Wu et al. 2022). More enticingly, results from prior theoretical and practical research have suggested that ZnO doped with appropriate transition metals can be used as diluted magnetic semiconductors (Sharma et al. 2012; Siddheswaran et al. 2013). Recently, transition metal oxide nanoparticles, such as zinc oxide (ZnO), titanium oxide (TiO₂), and tin oxide (SnO₂) that doped with a transition metal atoms have been studied in-depth for some applications. (Ansari et al. 2013; Wang et al. 2012). Researchers are interested in transition metals (TMs) doped with ZnO nanoparticles for multifunctional device applications. The optical properties of ZnO (NPs) are also influenced by doping a TM into ZnO (Farouk et al. 2020). Blue and UV light-emitting diodes, micro-electromechanical systems, surface acoustic wave devices, spintronic devices, transparent conducting electrodes, gas sensors, and other applications have all been made possible by chromium doped ZnO nanoparticles. (Ansari et al. 2012a; Jin et al. 2013). Chromium is a suitable transition metal with either a significant electron shell structure and a Cr³⁺ ionic radius (0.063 nm) that is similar to Zn²⁺ (0.074 nm). As a result, Cr³⁺ can be used as a simple doping agent in ZnO (NPs) (Jin et al. 2013). However, more researches of the Cr doped ZnO nanoparticle is required. That is because Cr in particular, has important magnetic, semiconductor, and optical characteristics (Ansari et al. 2012a). Several investigations have found that Cr-ions doped ZnO promotes the single-phase polycrystalline character of the wurtzite lattice (Kaur et al. 2015; Sirijan and Yongvanich 2014). This work aims to study the structural, optical, electrical and magnetic properties of ZnO nanoparticle doped with chromium that synthesize by co-precipitation method at room temperature, this method of preparation was rarely used in the previous publication.

2 Experimental details

Pure and Cr doped ZnO nanoparticles were prepared by the chemical co-precipitation method. All chemicals in the present work are commercial grade (LOBA Chemical) with high purity grade. Raw materials including Zinc acetate dehydrate [$\text{Zn}(\text{CH}_3\text{COO})_2 \cdot 2\text{H}_2\text{O}$, purity 98%], Chromium (III) Chloride hexahydrate [$\text{CrCl}_3 \cdot 6\text{H}_2\text{O}$, purity 93%], sodium hydroxide [NaOH , purity 93%], distilled water and ethanol. Pure and doped samples with different Chromium concentration with compositional formula of $\text{Zn}_{1-x}\text{Cr}_x\text{O}$, ($x=0, 0.06, 0.1, \text{ and } 0.14 \text{ wt } \%$) as ($\text{ZnO}, \text{ZnCr1}, \text{ZnCr2}, \text{ZnCr3}$) respectively.

The experimental system for the instruction of bulk and Cr- doped ZnO nanoparticles are as follows: for synthesis of blank ZnO nanoparticles, 21.950 g of Zinc Acetate was dissolved in 100 ml distilled water and magnetically stirred at room temperature (RT) to obtain homogenous solution, then 16 g of sodium hydroxide was dissolved in 100 ml distilled water. After that NaOH solution was supplemental drop wise acquire homogenized mixed solution, productive a white precipitate. The white powder was stirred at room temperature for 2 h. Afterward the solution was washed with ethanol and distilled water.

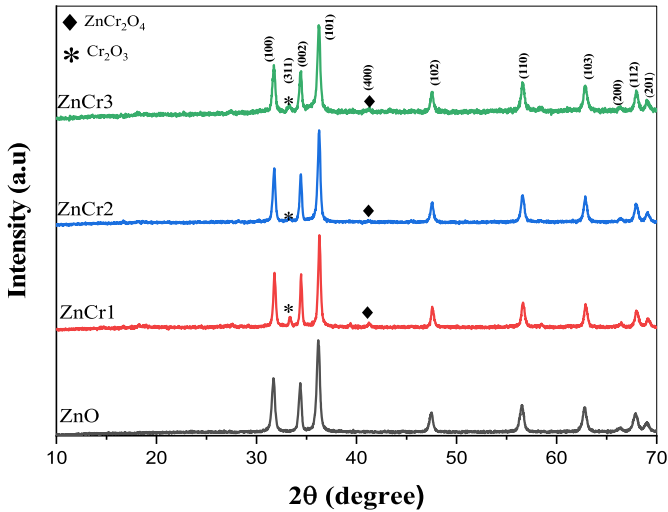
The white powder was dried at 70 °C for 3 h followed by further heating at 400 °C for 4 h. Then, the white powder was grind using agate mortar. For the synthesis, Cr-doped ZnO nanoparticles, the amount of $\text{CrCl}_3 \cdot 6\text{H}_2\text{O}$ [1.59 gm (0.06), 2.66 gm (0.1), and 3.7303 gm (0.14)] were dissolved in (20 ml) distilled water, and added to (19.755, 19.316, and 18.877 gm) of zinc acetate respectively for each sample dissolved in (80 ml) distilled water with continues stirring for 1 h. Chromium was added dropwise to zinc acetate solution with continuous stirring then (16 g) of sodium hydroxide which dissolved in (100 ml) distilled water was added dropwise to the homogenous mixture to get a white precipitate. Finally, the white solution precipitate was treated as above to gain Cr-doped ZnO samples. The prepared samples were then used for experimental characterization. The nanoparticles samples were examined by X-ray diffraction (XRD). FTIR technology is used to obtain information about the local structure of all prepared samples. Optical properties were detected by UV–Vis spectrophotometer. Dielectric measurements were examined with Novo- control high resolution alpha dielectric analyser in the frequency range 0.01 Hz to 10 MHz. Using Lakeshore-7404 vibrating sample magnetometer to measure magnetic properties.

3 Results and discussion

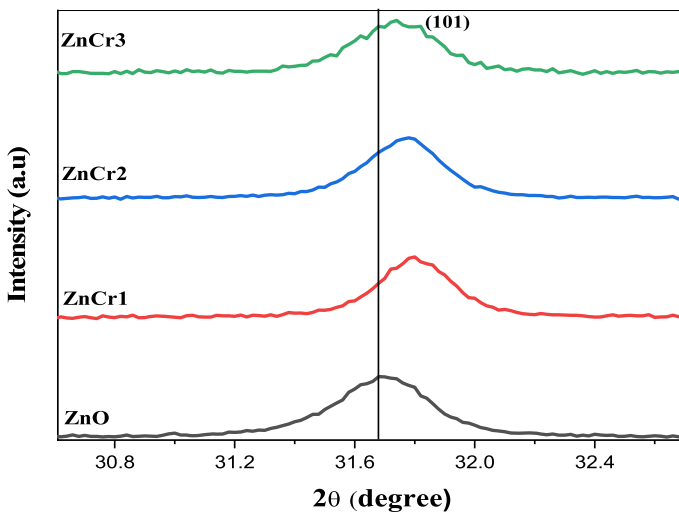
3.1 X-ray diffraction

X-Ray Diffraction (XRD) studied the crystalline phases formation of synthesized ZnO nanoparticles that doped with Cr-ions using $\text{CuK}\alpha$ radiation of wavelength 1.5406 Å in the range of (2θ) from 20 to 70°. Figure 1a showed that the blank sample of ZnO, and ZnO (NPs) doped with Chromium (III) Chloride, from Fig. 1a determine that the hexagonal wurtzite ZnO structure corresponding to the crystal planes (100), (002), (101), (102), (110), (103), (200), (112), (201) for blank ZnO nanoparticle. The two crystalline phases (311) and (400) were observed when added (CrCl_3) to ZnO lattice, it may be attributed to Cr_2O_3 and ZnCr_2O_4 (Zhao et al. 2020; Salahuddin et al. 2015).

According to the XRD results, there are observable secondary phases of ZnCr_2O_4 in doped samples within the detection limit of the XRD, and similarly a secondary phase of



(a) X-ray diffraction patterns of bulk ZnO and Cr doped ZnO nanoparticles with different Cr contents.



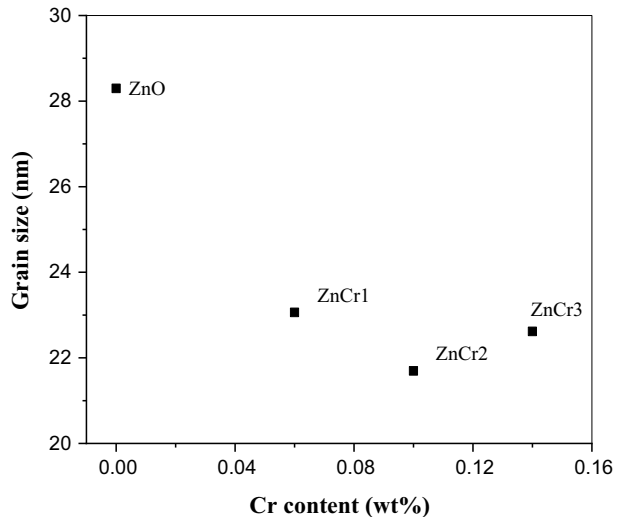
(b) Peak position shifts slightly to higher angle with increasing Cr concentration.

Fig. 1 **a** X-ray diffraction patterns of bulk ZnO and Cr doped ZnO nanoparticles with different Cr contents. **b** Peak position shifts slightly to higher angle with increasing Cr concentration

Cr_2O_3 appeared in all dopant samples, where Duan et al., reported a similar results (Duan et al. 2010). The prominent peak (101) that showed a slight shift toward a higher angle 2θ about 0.1° for all doped samples compared with the pure ZnO as shown in Fig. 1b, this shift has nearly the same value as dopant value of Cr was increased gradually up to 0.14 wt

Table 1 Calculated values of crystallite size, dislocation density (δ), and the micro-strain (ϵ) for bulk ZnO and Cr doped ZnO nanoparticles

Cr doping (x) wt%	r(nm)	$\delta \times 10^{-3}$	Micro-strain ($\epsilon \times 10^4$)
0	28.29	1.2494	0.000588
0.06	22.95	1.8974	0.000402
0.1	18.97	1.4826	0.000395
0.14	21.34	2.1958	0.000443

Fig. 2 Variation of crystal size with Cr doping content

%. This can be ascribed as the Cr ions are successfully substituted Zn ions in ZnO lattice, because that the ionic radii value of Cr^{3+} (0.615 Å) is smaller than Zn^{2+} ion (0.74 Å), this may be the reason of slightly shift to a higher value of 2θ (Bhargava et al. 2010).

Small changes in diffraction angle due to Cr-doped ZnO (NPs) may be discovered by variances in the lattice constant when compared with bulk ZnO. As a result, the predicted values of the lattice parameter changed slightly, owing to the amount of NaOH employed in the sample preparation. To reach some valuable information regarding high dopant content some calculations have done. The average crystallite size was calculated by using Scherer's equation (Habib et al. 2018).

$$r = \frac{K\lambda}{\beta \cos \theta} \quad (1)$$

where r is the average crystallite size in nanometers (nm), K is a constant (0.9), λ is the wavelength of incident Cu $K\alpha$ radiation = 1.54060 Å, β is the whole width at half maximum intensity of the different peaks in radians, and θ is the diffraction angle. Table 1 shows the crystallite size results for pure ZnO (NPs) and Cr doped ZnO nanoparticles.

It could be seen that the variation of crystallite size which obtained from Eq. (1) with Cr concentration exhibited reduction from 28.29 to 18.97 nm as Cr concentration increased from (0.06 to 0.1 wt %) and increased once more by increasing the Cr content to 0.14 wt % as shown in Fig. 2. One of the reasons of the reduction in particle size may be due to the increase in Cr content that prevent particle growth, grain boundary

movement should be impeded (Kelsall et al. 2006). This can provide an explanation for prevention to motion of the grain barriers that changed into stated by Zener pinning (Wörner and Hazzledine 1992). While the moving barriers attached the zinc interstitial and substituted Cr ions, they will follow a retarding pressure between the barriers. If the retarding forces that have been produced is more than the driving forces for grain increase the particle size cannot grow any longer (Wang et al. 2008).

Also, it can be assumed that Cr^{3+} ions caused the decrease of lattice parameters because the smaller ionic radius which is already mentioned (Bhargava et al. 2010). Meanwhile, the increase in the particle size that observed at $x=0.14$ wt % may be due to the possibility of some residence chromium atoms on the octahedral interstitial site, as a strong preference of Cr for the octahedral coordinate instead of the tetrahedral one with oxygen (Hassan et al. 2015a). The micro strain (ϵ) and dislocation density (δ) were calculated for all the prepared samples by the following formula (Murugan et al. 2018; Srinivasulu et al. 2017):

$$\epsilon = \frac{\beta}{4 \tan \theta} \quad (2)$$

$$\delta = \frac{1}{r^2} \quad (3)$$

where (δ) is the number of dislocation lines per unit volume present in the synthesized nanoparticles, the values of r , δ and ϵ is depicted in Table 1, The high value of δ for all doped samples compared with the bulk one may be due to the formation of crystal defects round the dopant ions, and these defects caused change of the stoichiometry of the doped samples. The micro-strain value of the bulk sample showed high value than that of doped sample.

While these values showed decreasing value with increasing the Cr content. These results may let us say that compression stress state is transformed to tensile stress (Karthika and Ravichandran 2015). The lattice parameters (a), (c) and unit cell volume for ZnO phase were calculated for all the prepared samples. The equation of inter planer spacing for a tetragonal unit cell is given by Habib et al. (2019)

$$\frac{1}{d^2} = \frac{3}{4} \left(\frac{h^2 + hk + k^2}{a^2} \right) + \frac{l^2}{c^2} \quad (4)$$

where d is the inter-planar spacing and the h , k and l are the miller indices. d - Spacing is given by Braggs law:

$$n\lambda = 2d \sin \theta \quad (5)$$

where $\lambda = 1.5406 \text{ \AA}$, θ is the diffraction angle. $n=1$ (order of diffraction).

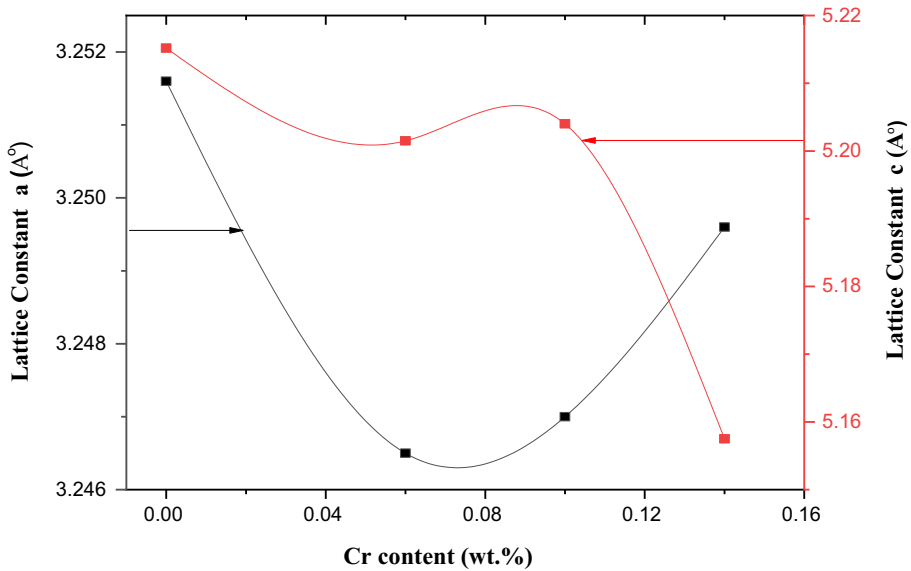
The unit cell volume (V) of the hexagonal structure of the ZnO (NPs), is calculated from Eq. (6). (Habib et al. 2019).

$$V = \frac{\sqrt{3}}{2} ac^2 \quad (6)$$

Along the c -direction the bond length of Zn–O is given by Sangeetha et al. (2015)

Table 2 Lattice parameters, u parameter, cell volume and bond length of Blank ZnO and Cr doped ZnO nanoparticles

Cr content (wt %)	a (Å)	c (Å)	c/a	u	Cell volume (Å ³)	Bond length (Å)
0	3.2516	5.2152	1.603	0.3795	47.751	2.27
0.06	3.2465	5.2015	1.602	0.3798	47.476	2.26
0.1	3.247	5.204	1.602	0.3797	47.51	2.26
0.14	3.2496	5.1575	1.587	0.3823	47.164	2.24

**Fig. 3** Lattice parameters (a, c) vs Cr concentration

$$l = \sqrt{\left(\frac{a^2}{3} + \left(\frac{1}{2} - u\right)^2 c^2\right)} \quad (7)$$

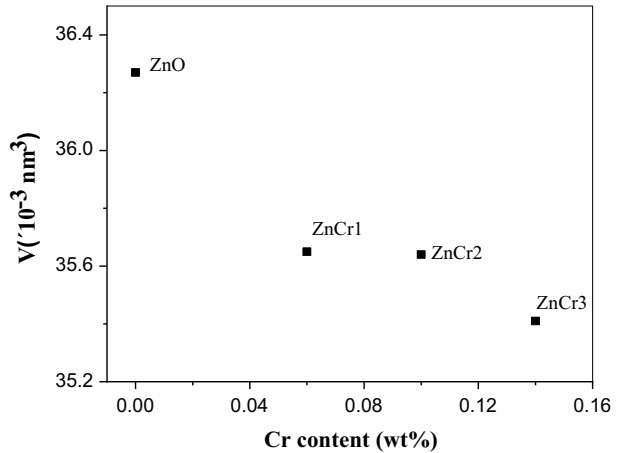
The positional parameter (u) which is an important variable in calculating the Zn–O bond length is given by Eq. (8).

$$u = \frac{1}{3} \left(\frac{a^2}{c^2}\right) + \frac{1}{4} \quad (8)$$

The values of lattice constants, unit cell volume, bond length and (u) are presented in Table 2. It is remarkable to note that the values of (a) and (c) are slightly decreasing for all doped samples as Cr contents were increased. Firstly, decreased as Cr concentration is increased (from 0.06 to 0.1 wt %) and then increased for higher Cr content (0.14 wt %) as shown in Fig. 3.

The decrease of the lattice constants and the slight shift in the XRD peaks is attributed to the incorporation of Cr doping within the ZnO matrix, which causes a small misfit due

Fig. 4 Evolution of unit cell volume V of hexagonal wurtzite phase of $Zn_{1-x}Cr_x$ as a function of x



to the difference of ionic radius of Cr ion and Zn ion. This result was also supported by the decrease in the unit cell volume with increasing of Cr content as shown in Fig. 4.

From Table 2 there is a relationship between the (c/a) ratio and the (u) parameter. The (c/a) ratio decreases as the (u) parameter increased, so that these tetrahedral lengths remain almost constant, and the tetrahedral angles are distorted due to extensive polar interactions. The length of the Zn–O bond with the lattice parameters has been found to decrease, confirming the decreasing in particle size for all doped samples (Ahmed et al. 2012).

3.2 FTIR analysis

The FTIR spectroscopy technique was used to investigate the chemical bonding and existence of functional groups in the produced samples. Many elements, including chemicals, influenced the increasing number of peaks and bond positions. Structures, modulation, and crystal structure, etc. Figure 5 indicates the FTIR spectra of bulk and Cr doped ZnO nanopowders prepared by co-precipitation method. The results exhibited the formation of the wurtzite ZnO structure in ZnO and Cr doped ZnO nanoparticles in the wave number range from 4000 to 400 cm^{-1} .

The broad absorption bands between 2700 cm^{-1} and 3500 cm^{-1} are assigned to stretching vibration of hydroxyl groups of water in Zn–O lattice, indicating of presence of H_2O absorbed on the surface of nanocrystals in the prepared ZnO nano-powders (Reddy et al. 2011; Zahabi et al. 2022). Bending vibration H–O–H is observed in the range between 1636 cm^{-1} to 1655 cm^{-1} for all samples due to the little amount of water in ZnO nanoparticles (Dasari et al. 2018). The other peaks at around 1500 and 1540 cm^{-1} were attributed to C=C bonds this may be due to the carbonyl groups of the carboxylate ions which may remain adsorbed at the surface of nanoparticles (Saravanana et al. 2012). The peaks appeared in the range 1000 – 1500 cm^{-1} may be indicated to C=O symmetric and asymmetric stretching (Shah et al. 2020). The FTIR spectra, in between the region 1000 – 400 cm^{-1} as a most complex and reveals a good picture about ZnO host, all spectra can be deconvoluted around this region. As shown in Fig. 6 Stretching modes of Zn–O–Cr were observed around 833 cm^{-1} to 908 cm^{-1} that confirm the presence of defects that resulted from oxygen vacancies which existing in the system due to Cr incorporation in the ZnO lattice (Bodke and Dole 2015). This band confirms that Cr cations have been occupied in the

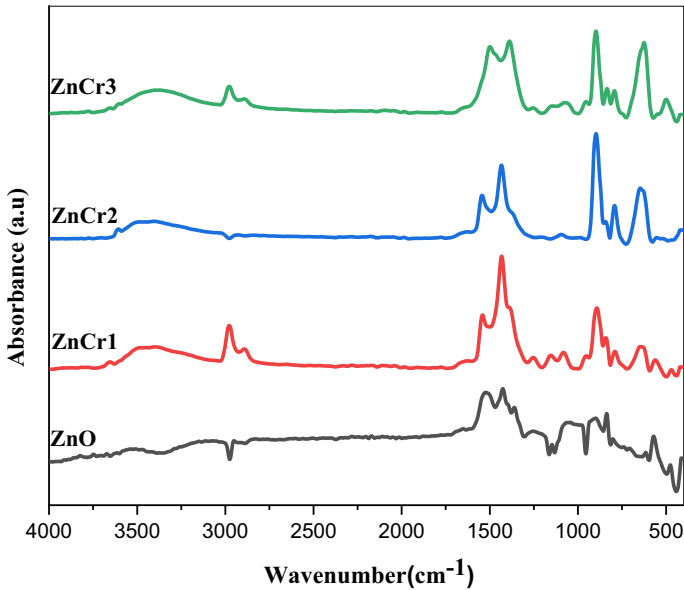


Fig. 5 FT-IR spectra of bulk ZnO and Cr doped ZnO nanoparticles

ZnO (NPs) matrix, which matches the XRD results. The shoulder band at 612 cm^{-1} may be assigned to the stretching vibration of Zn–O bonds in octahedral coordinate (Hassan et al. 2015a). The increase of Cr^{+3} doping to ZnO nanoparticles caused the band around 612 cm^{-1} to shift toward the higher wavenumber 640 cm^{-1} (in Cr-rich sample), which reveals an increase in the strength of Zn–O bond, that is may attributed to optical phonon confinement by nanostructures, it is highly possible because the nanostructures in our samples are bigger in size than the Bohr exciton radius in ZnO (2.3 nm), this in turn caused the observed increase in its height this is may be due to the stretching vibration of ZnO in the tetrahedral and octahedral coordination respectively may be caused the intensity increase as the Cr content was increased according to the existence of defects states that surrounding to Cr ions (42–43), While, the absorption wide range band $470\text{--}570\text{ cm}^{-1}$ may be due to the stretching vibrational mode of vibrational Zn, and Cr cations (Bodke and Dole 2015; Farag et al. 2022).

3.3 Optical properties

UV–Vis absorption spectroscopy with high performance is unique powerful techniques to investigate the optical characteristic of semiconductor NPs. The band gap of a semiconductor materials changes with the formation of the impurities and Crystal defects (Hassan et al. 2014), the absorbance may be differ depending upon some factors such as particle size, oxygen deficiency, and defects in grain boundary (Soitah, et al. 2010). The UV–Vis absorption spectrum of bulk ZnO and Cr doped ZnO nanoparticle recorded in the range 290–900 nm at room temperature, the nano-powders were dispersed in glycerin. As shown in Fig. 7 the absorption spectra of bulk ZnO and different Cr concentration doped ZnO nano-particle recorded in the range 290–900 nm. It can be seen from

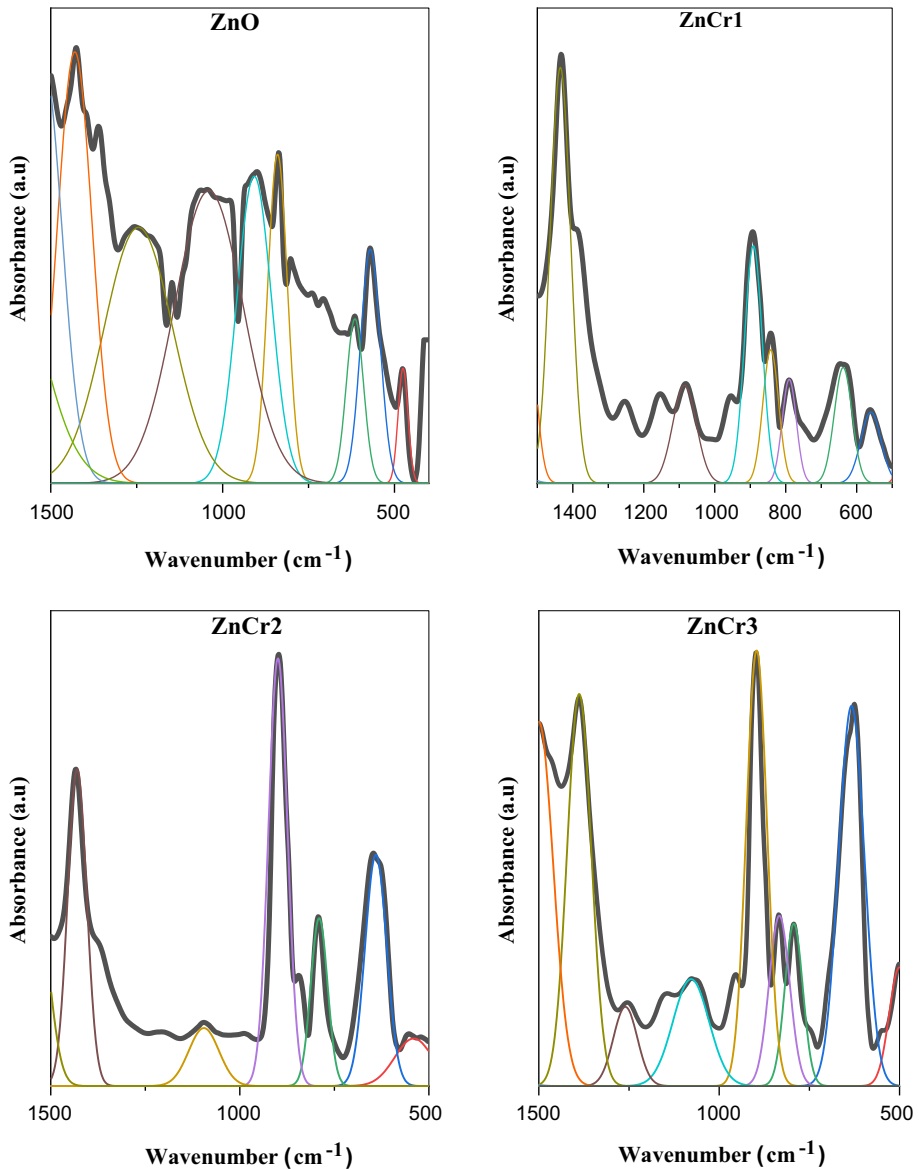


Fig. 6 The band deconvolution of FT-IR spectra for all prepared samples

Fig. 7 bulk ZnO nano-powder showed slight absorbance around 371 nm in the visible region whereas all doped ZnO nanoparticle samples have little absorbance at wavelength about 373 nm, this slight shift is due to doping of Cr ions which may be increase the electron concentration that cause more widen band gab of ZnO nanoparticles (Zak et al. 2011). The incorporation does shift toward longer wavelengths (red shift), this shift may be due to spin sp-d exchange interactions between band electrons and the localized d electrons of the Cr³⁺ cation (Wang et al. 2013). Tauc's relation is used to

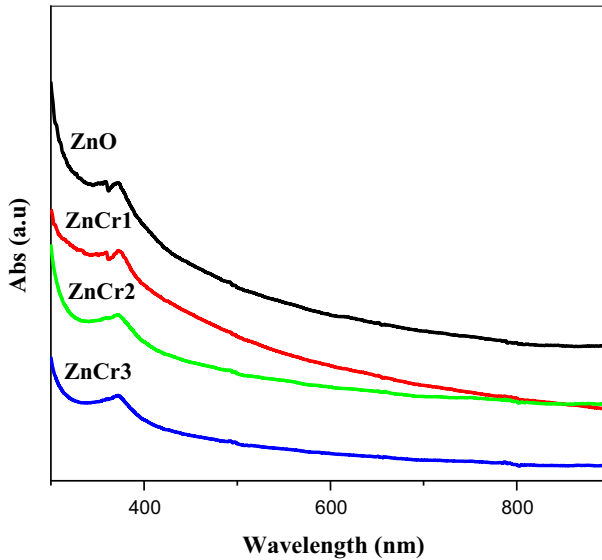


Fig. 7 UV–Vis spectra for all the prepared samples

compute the optical band gap energy of pure ZnO and Cr doped ZnO nanoparticles for direct energy band gap (Sadeq and Ibrahim 2021):

$$(\alpha h\nu)^n = A(h\nu - E_g) \quad (9)$$

where (α) is the absorption coefficient, (A) is a constant, and E_g is the optical band gap and $n=1/2$ for the allowed direct energy band gap, and $n=2$ for indirect band gap materials, where $n=3/2$ for a forbidden direct energy gap for semiconductor nanoparticles (Sayyed et al. 2022; Ibrahim and Sadeq 2021). The calculation values of band gap are given in Table 3. The most satisfactory results were obtained by plotting the quantity $(\alpha h\nu)^2$ as a function of $(h\nu)$, as shown in Fig. 8. The values of (E_g) can be obtained by extrapolating the linear fit and the intercept of this linear region on the energy axis at $(\alpha h\nu)^2=0$ gives the band gap. From inset Fig. 8, it is exhibited that the optical band gap (E_g) values increased with increasing Cr content from 0 to 0.14 wt %. The increase in energy band gap may be due to the increase of the charge carrier's concentration that block the lowest state in the conduction band, this behavior is well known as Burstein–Moss effect (Sahal et al. 2008). The Fermi level rises into the conduction bands as charge carrier concentrations grow, and the rise in charge carrier concentration increases the optical energy band gap. This increase

Table 3 Optical band gap energy of ZnO and Cr doped ZnO nanoparticle

Cr doping wt%	Optical band gap energy E_g (eV)
0	3.84
0.06	3.91
0.1	3.98
0.14	4.02

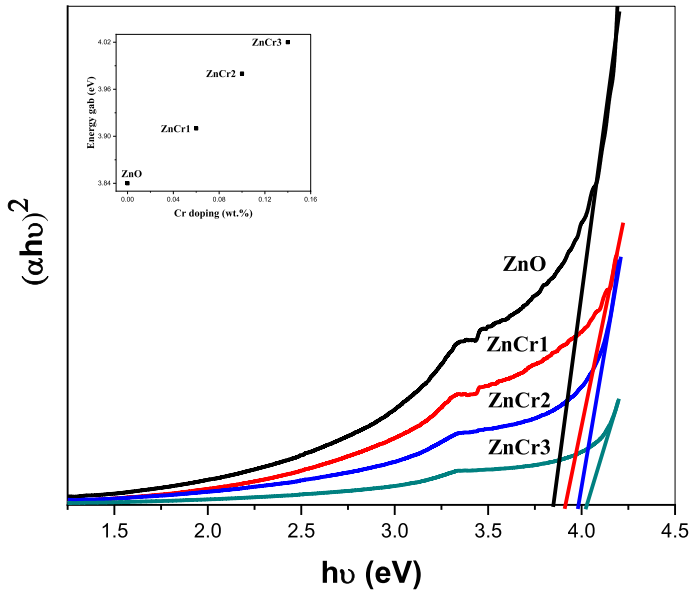


Fig. 8 Plots of $(\alpha h\nu)^2$ versus photon energy ($h\nu$) for all prepared samples

in band gap with increasing Cr content could be ascribed to the size quantization effect relative to the size of ZnO nanoparticles (Shan and Yu 2004).

3.4 Dielectric characteristics

3.4.1 Dielectric constant

The nano ZnO matrix has polar molecule with permanent dipole moment affected by the external electric field. Its complex dielectric permittivity ϵ^* is known by equation (Hasan et al. 2015b):

$$\epsilon^* = \epsilon' - j\epsilon'' \quad (10)$$

where ϵ' is the real part of dielectric permittivity that gives the stored energy of a material, and the ϵ'' is the imaginary part of dielectric permittivity or the complex part of ϵ , that means the dissipated energy that given from polarization and ionic conduction (Das et al. 2017). Frequency dependence on the dielectric constant at 298 K of temperature for bulk ZnO (NP_s) and Cr doped samples appear in Fig. 9. The values of ϵ' for the pure ZnO (NP_s) and doped with 0.06, 0.1 wt % Cr was. (0.0280×10^4) for $\log(f) = 0.1$ Hz. Moreover, it is observed that the dielectric constant shows increasing values as Cr content was increased at the lower frequencies range, while it gives a high value 1.8×10^5 for $\log(f)$ equal 0.2 Hz at Cr concentration (0.14wt %), while it is decreased down to 3.3×10^3 at $\log(f)$ equal 100 Hz. Then it became stable from 100 Hz up to 10^7 Hz likewise the other prepared samples. This behavior is related to the polarization mechanism and the relaxation process that formally occur in the nanostructured materials. The Maxwell–Wagner interface model, which is also in excellent accord with phenomenological Koops' theory of double

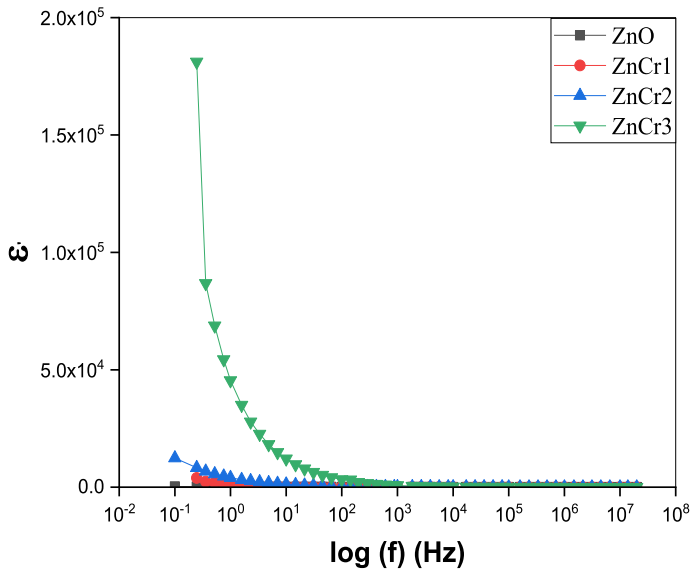


Fig. 9 Variations of dielectric constant vs. $\log(f)$ for ZnO:Cr nanoparticles at 298 K

homogeneity structure (Das et al. 2017), may be used to show the dielectric distribution of oxide nanoparticles in general. The charge carriers accumulated at the less conductive grain borders that were more influenced by applied electric field in this model according to the poor conductivity grain boundaries (Hassan et al. 2015a). These charge carrier's accumulations procedure on the edges of the isolating grain boundaries, resulting in strong polarizability, which leads to substantial polarization and a high dielectric constant at lower frequencies (Bhakta and Chakrabarti 2019). The significant value of the dielectric constant at lower frequencies less than (10^2 Hz) might be attributable to different phenomena in the lattice and at the grain boundary of ZnO nanoparticles, such as oxygen vacancies and grain boundaries defects (Das et al. 2018). Furthermore, the greatest value of ϵ' at low frequencies may be owing to the combined contribution of many forms of polarization, such as ionic, electronic, interpolated, and dipolar (Das et al. 2018). According to the polarization process in compounds based on ZnO, the sample of 0.14 Cr (wt %) exhibits the lowest value with increasing frequency. At higher applied frequencies more than 100 Hz, the electric dipoles cannot follow the applied electric field so ϵ' value became constant at higher frequencies (Belkhaoui et al. 2019a). The lag between the frequency of oscillations of the dipole and that of the external electric field may produce a reduction in the number of dipoles contributing to the polarization process and/or the inability of dipoles to respond fast (Tabib et al. 2015). The high value of dielectric constant at temperature 298 K makes the 0.14 Cr wt % sample a promising sample for charge storage applications.

3.4.2 Dielectric loss ($\tan\delta$)

The dielectric loss occurs when the polarization of the dielectric material is not able to follow the variation of the applied electric field. The dielectric loss is calculated by the relation (Tabib et al. 2015):

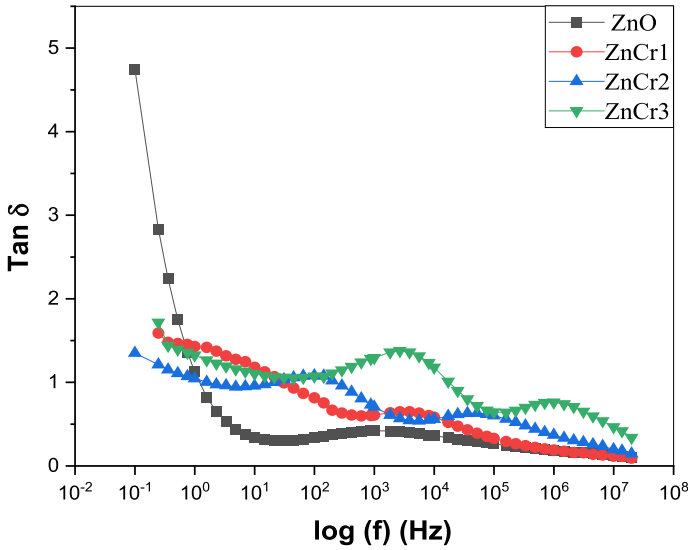


Fig. 10 Variations of dielectric loss $\tan(\delta)$ versus $\log(f)$ for bulk ZnO NPs and that doped with Cr at 298 K

$$\tan\delta = \frac{\epsilon''}{\epsilon'} \tag{11}$$

Figure 10. Showed the variation of $\tan \delta$ as a function of frequency at 298 K, it is evident that the dielectric loss decreases as the frequency of ZnO and Cr-doped ZnO nanoparticles was increased. The value of $\tan \delta$ is found to be high at lower frequencies, while becomes lower at higher frequencies. The decreasing value of dielectric loss with increasing the applied frequency may be due to the domain wall resonance (Samkaria and Sharma 2013). Figure 10. Showed a hump that displayed in each $\tan(\delta)$ with $\log(f)$ relation which may be indication to relaxation peak. This hump happens when the value of localized charge carrier’s frequency approaches that of the applied ac electric field (Samkaria and Sharma 2013). In general, it is obvious that the value of $\tan(\delta)$ decreased with increasing the Cr concentration up to 0.14 wt %. While the low values of dielectric loss at higher frequencies make it promising sample for nonlinear optical applications (Samkaria and Sharma 2013). In addition, materials with low dielectric constant values and dielectric loss at higher frequencies are suitable candidates for high frequency operating devices (Khan et al. 2018b).

3.4.3 Acconductivity

The ac conductivity (σ_{ac}) for each sample is calculated from the following equation (Hasan et al. 2012), where ω the angular frequency and ϵ_0 is the permittivity of free space ($8.854 \cdot 10^{-12}$ F/m).

$$\sigma_{ac} = \epsilon' \epsilon_0 \omega \tan \delta \tag{12}$$

Figure 11 showed the variation of ac conductivity (σ_{ac}) with the frequency of pure ZnO and Cr doped ZnO nanoparticles measured at 298 K. The (σ_{ac}) values exhibit increasing values along with frequency especially at higher frequencies. This is refers to the enhancement of migration of the electrons (Ansari et al. 2012b). It is clear from

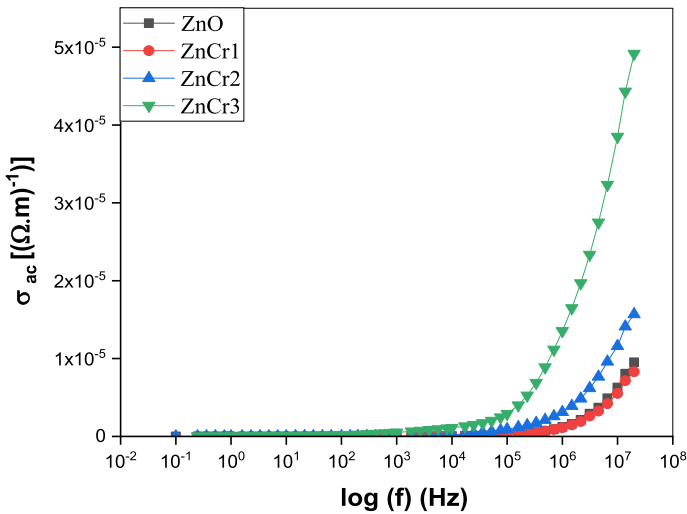


Fig. 11 Variations of AC conductivity versus $\log(f)$ for ZnO: Cr doped ZnO nanoparticles at 298 K

Fig. 11 that the increase of (σ_{ac}) is nearly coincident at lower and middle frequencies, then it is increased rapidly and the relation of different samples became dispersed at frequencies from 10^4 to 10^7 Hz. This means that the (σ_{ac}) value is more frequency-dependent as the frequency increased. This variation of (σ_{ac}) between the two ranges of frequency-independent into the frequency-dependent indicates the conductivity relaxation phenomenon (Ansari et al. 2012b).

Furthermore, the gradual increase of (σ_{ac}) with frequency can be explained in terms of the Maxwell–Wagner interface model (Khan et al. 2018b), that is due to the interfaces or grain boundaries represents a potential barrier against the flow of the charge carriers then these charges behave like particles in a box (Gürbüz and Okutan 2016). At low frequencies range insignificant increase in conductivity may be due to some of the charge carriers that flow through tunnel in the potential barrier giving a little rise in conductivity (Belkhaoui et al. 2019b). As the frequency of the applied electric field increased the charge carriers get enough energy to overcome the potential barrier, which promotes intensively the conductivity at higher frequency (Khan et al. 2018b; Ansari et al. 2012b; Ashokkumar and Muthukumaran 2015). On the other hand, it can be seen from Fig. 11 that the (σ_{ac}) increases with high doping concentration except the 0.06 wt % Cr doping sample which showed a little decrease of the electrical conductivity. This result may be referred to the defects that presented due to Cr doping that took place in zinc interstitials and oxygen vacancies in the ZnO nanoparticles host matrix. These defects caused isolation at the grain boundaries which acts as a block to the flow of charge carriers (Belkhaoui et al. 2019a, Ansari et al. 2012b, Belkhaoui et al. 2019b). This caused reduction of conductivity of the low Cr dopant concentration sample. Also, the electrical conductivity increased with increasing of Cr concentration (0.1 wt % to 0.14 wt %) in the ZnO (NPs) matrix this is refer to the fact that the increase of Cr concentration raises the hopping process of Cr ions between $\text{Cr}^{+2} \rightarrow \text{Cr}^{+3}$ that predominated over charge carriers blocking effect (Belkhaoui et al. 2019b). These results make us suggesting that Cr doped ZnO nanoparticles may be considered a promising candidate for high-energy storage devices. Over and above, the improved electrical conductivity

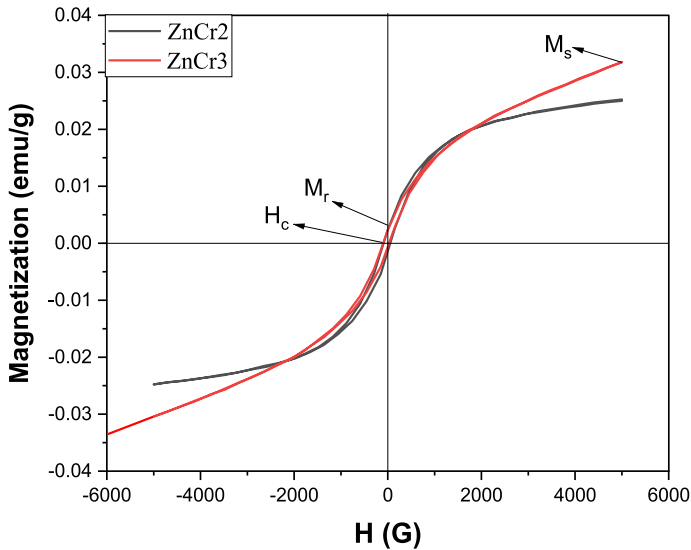


Fig. 12 Hysteresis loops M-H curve of two selected samples ZnCr2 and ZnCr3 at room temperature

Table 4 Saturation magnetization, remanent magnetization and coercivity for selected sample of ZnCr2, ZnCr3

Samples	Saturation magnetization (M_s) emu/g	Remanent magnetization (M_r) emu/g	Coercivity (H_c) G
ZnCr2	25.02×10^{-3}	2.5×10^{-3}	89.5
ZnCr3	33.10×10^{-3}	2.3×10^{-3}	100

caused an increase in the electron transmission which is important for gas and humidity sensing (Tabib et al. 2015; Khan et al. 2019).

3.5 Magnetic measurements

The magnetic hysteresis (M-H) loops obtained by VSM at room temperature for selected samples of $Zn_{1-x}Cr_xO$ ($x=0.1$ and 0.14) using a magnetic field (H) in the range of ± 5000 G. Figure 12 showed (M-H) loop of both selected samples were exhibited a ferromagnetic behavior at room temperature. The observed magnetic parameters such as saturation magnetization, remanent magnetization and coercivity displayed in Table 4. It can be seen from Table. 4 that the saturation magnetization increased with the increase of Cr content as well as the coercivity while the remanent is decreased slightly. These results nearly confirmed the results of B. Babu et al. (Babu et al. 2014). The expected two reasons for ferromagnetism that appeared in our data in Table 4, the first one may be due to the number of defects that mentioned in XRD results and oxygen vacancies (Liu et al. 2009). The second reason may be according to the interactions of transition metal (Cr) and spin moments of oxygen ions (Sanad et al. 2019). The obtained results make Cr-doped ZnO (NPs) samples promising for the spin-based electronic devices.

4 Conclusion

Pure ZnO and ZnO nanoparticles doped with Cr were synthesized via Co-precipitation method with different doping concentrations. The synthesized $Zn_{1-x}Cr_xO$ nanoparticles were characterized using XRD, FTIR Spectroscopy, UV–Vis Spectrophotometry, ac measurement and VSM. XRD showed the wurtzite phase formation in all Cr doped samples with two crystalline phases ($ZnCr_2O_4$ and Cr_2O_3) have been observed. The particle size for the blank sample is equal (28.29 nm) while it decreased in the Cr doped samples. A little shift in the position of XRD peaks and changes in cell parameters, bond length, unit cell volume and the micro-strain suggested the substitution of Cr into Zn–O lattice. FTIR analysis revealed the presence of Zn–O and Zn–Cr–O bonds. The optical absorption spectra showed a red shift due to the sp-d exchange interactions between band electrons and the localized d electrons of the Cr^{3+} ions in the absorption band edge with increasing Cr concentration which leads to increasing of optical band gap from 3.85 to 4.02 eV. The dielectric constant ϵ' exhibited decreasing values at high frequencies and increasing values at low frequencies along with increment Cr concentration especially sample of 0.14 wt % Cr content, and dielectric loss $\tan(\delta)$ showed increasing values at low frequencies and decreasing values as Cr doping concentration was increased along with the higher frequencies. The increase in ac conductivity (σ_{ac}) values at higher frequencies were explained in terms of the Maxwell–Wagner interface model. The obtained results of Cr doped ZnO nanoparticle let us considered these samples are potential candidate for different applications such as high-energy storage devices, high frequency operating devices and nonlinear optical applications. In addition, the improved dielectric constant at room temperature makes the doped sample of 0.14 wt % Cr doping is a promising sample for charge storage applications. Samples doped with ($x=0.1$ and 0.14 Cr wt %) showed ferromagnetic behavior at room temperature. Moreover these magnetic results are also applicable for the spin-based electronic devices.

Acknowledgements The authors are grateful to Dr. Mohamed El-Okr, professor of solid state physics at the Faculty of Science in Cairo for Boys, Al-Azhar University, Cairo, Egypt, who had the initial idea for this research.

Authors' contributions All authors contributed to the study conception and design. Samples preparation, data collection and analysis were performed by prof. M.Y. Hassaan, Dr. F.M. Ebrahim, Dr. K. Adly. The initial draft of the manuscript was written by Dr. Nasser Moussa and all authors commented on previous versions of the manuscript. All authors read and approved the final manuscript.

Funding Open access funding provided by The Science, Technology & Innovation Funding Authority (STDF) in cooperation with The Egyptian Knowledge Bank (EKB). Not applicable.

Data availability Not applicable.

Declarations

Conflict of interests The authors have no relevant financial or non-financial interests to disclose.

Ethical approval and consent to participate Not applicable.

Human and animals rights Not applicable.

Informed consent Not applicable.

Consent for publication Not applicable.

Open Access This article is licensed under a Creative Commons Attribution 4.0 International License, which permits use, sharing, adaptation, distribution and reproduction in any medium or format, as long as you give appropriate credit to the original author(s) and the source, provide a link to the Creative Commons licence, and indicate if changes were made. The images or other third party material in this article are included in the article's Creative Commons licence, unless indicated otherwise in a credit line to the material. If material is not included in the article's Creative Commons licence and your intended use is not permitted by statutory regulation or exceeds the permitted use, you will need to obtain permission directly from the copyright holder. To view a copy of this licence, visit <http://creativecommons.org/licenses/by/4.0/>.

References

- Ahmed, F., Kumar, S., Arshi, N., et al.: Morphological evolution between nanorods to nanosheets and room temperature ferromagnetism of Fe-doped ZnO nanostructures. *Cryst. Eng. Comm.* **14**, 4016–4026 (2012)
- Ansari, S.A., Nisar, A., Fatma, B., et al.: Temperature dependence anomalous dielectric relaxation in Co doped ZnO nanoparticles. *Mater. Res. Bull.* **47**, 4161–4168 (2012a)
- Ansari, S.A., Nisar, A., Fatma, B., et al.: Investigation on structural, optical and dielectric properties of Co doped ZnO nanoparticles synthesized by gel-combustion route. *Mater. Sci. Eng. B* **177**, 428–435 (2012b)
- Ansari, S.A., Khan, M.M., Kalathil, S., et al.: Oxygen vacancy induced band gap narrowing of ZnO nanostructures by an electrochemically active biofilm. *Nanoscale* **5**(19), 9238–9246 (2013)
- Arora, A.K., Devi, S., Jaswal, V.S., et al.: Synthesis and characterization of ZnO nanoparticles. *Orient. J. Chem.* **30**, 1671–1679 (2014)
- Ashokkumar, M., Muthukumaran, S.: Effect of Ni doping on electrical, photoluminescence and magnetic behavior of Cu doped ZnO nanoparticles. *J. Lumin.* **162**, 97–103 (2015)
- Babu, B., Manjari, V.P., Aswani, T., et al.: Structural, optical and magnetic properties of Cr³⁺ doped ZnO nanopowder. *Indian. J. Phys.* **88**, 683–690 (2014)
- Belkhaoui, C., Mzabi, N., Smaoui, H.: Investigations on structural, optical and dielectric properties of Mn doped ZnO nanoparticles synthesized by co-precipitation method. *Mater. Res. Bull.* **111**, 70–79 (2019a)
- Belkhaoui, C., Mzabi, N., Smaoui, H., et al.: Enhancing the structural, optical and electrical properties of ZnO nanopowders through (Al + Mn) doping. *Results Phys.* **12**, 1686–1696 (2019b)
- Bhakta, N., Chakrabarti, P.K.: XRD analysis, Raman, AC conductivity and dielectric properties of Co and Mn co-doped SnO₂ nanoparticles. *Appl. Phys. A* **73**, 125–135 (2019)
- Bhargava, R., Sharma, P.K., Kumar, S., et al.: Consequence of doping mediated strain and the activation energy on the structural and optical properties of ZnO: Cr nanoparticles. *J. Solid. State Chem.* **183**, 1400–1408 (2010)
- Bodke, M.R., Dole, B.N.: Crystallographic, optical and morphological study of Cr doped ZnO nanocrystals. *J. Mater. Sci. Photon* **121**, 185–191 (2015)
- Das, S., Das, S., Sutradhar, S.: Effect of Gd³⁺ and Al³⁺ on optical and dielectric properties of ZnO nanoparticle prepared by two-step hydrothermal method. *Ceram. Int.* **43**, 6932–6941 (2017)
- Das, S., Bandyopadhyay, A., Das, S., et al.: Defect induced room-temperature ferromagnetism and enhanced dielectric property in nanocrystalline ZnO co-doped with Tb and Co. *J. Alloys. Compd.* **731**, 591–599 (2018)
- Dasari, M.P., Godavarti, U., Mote, V.: Structural, morphological, magnetic and electrical properties of Ni-doped ZnO nanoparticles synthesized by co-precipitation method. *Process. Appl. Ceram.* **12**, 100–110 (2018)
- Duan, L.B., Zhao, X.R., Liu, J.M., et al.: Room-temperature ferromagnetism in lightly Cr-doped ZnO nanoparticles. *Appl. Phys A* **99**, 679–683 (2010)
- Farag, M.A., Ibrahim, A., Hassaan, M.Y., Ramadan, R.M.: Enhancement of structural and optical properties of transparent sodium zinc phosphate glass–ceramics nano composite. *J. Aust. Ceram. Soc.* **58**(2), 653–661 (2022). <https://doi.org/10.1007/s41779-022-00716-3>
- Farouk, M., Samir, A., Ibrahim, A., et al.: Raman, FTIR studies and optical absorption of zinc borate glasses containing WO₃. *Appl. Phys. A* (2020). <https://doi.org/10.1007/s00339-020-03890-y>
- Gürbüz, O., Okutan, M.: Structural, electrical, and dielectric properties of Cr doped ZnO thin films: role of Cr concentration. *Appl. Surf. Sci.* **387**, 1211–1218 (2016)
- Habib, I.Y., Kumara, N.T.R.N., Lim, C.M., et al.: Dynamic light scattering and zeta potential studies of ceria nanoparticles. *Solid State Phenom.* **278**, 112–120 (2018)

- Habib, I., Tajuddin, A.A., Noor, H.A., et al.: Enhanced Carbon monoxide-sensing properties of Chromium-doped ZnO nanostructures. *Scientific Reports* (2019). <https://doi.org/10.1038/s41598-019-45313-w>
- Hassan, M.M., Ahmed, A.S., Chaman, M., et al.: Structural and frequency dependent dielectric properties of Fe³⁺ doped ZnO nanoparticles. *Mater. Res. Bull.* **47**, 3952–3958 (2012)
- Hassan, M.M., Khan, W., Azam, A., et al.: Effect of size reduction on structural and optical properties of ZnO matrix due to successive doping of Fe ions. *J. Lumin.* **145**, 160–166 (2014)
- Hassan, M.M., Khana, W., Azam, A., et al.: Influence of Cr incorporation on structural, dielectric and optical properties of ZnO nanoparticles. *J. Ind. Eng. Chem* **21**, 283–291 (2015a)
- Hassan, M.M., Khan, W., Azam, A., et al.: Influence of Cr incorporation on structural, dielectric and optical properties of ZnO nanoparticles. *J. Indust. Engin. Chemi* **21**, 283–291 (2015b)
- Ibrahim, A., Sadeq, M.S.: Influence of cobalt oxide on the structure, optical transitions and ligand field parameters of lithium phosphate glasses. *Ceram. Int.* **47**, 28536–28542 (2021)
- Jin, X., Götz, M., Wille, S., et al.: A novel concept for self-reporting materials: stress sensitive photoluminescence in znO tetrapod filled elastomers. *Adv. Mater.* **25**, 1342–1347 (2013)
- Karthika, K., Ravichandran, K.: Tuning the microstructural and magnetic properties of ZnO nanopowders through the simultaneous doping of Mn and Ni for biomedical applications. *J Mater Sci. Technol.* **31**, 1111–1117 (2015)
- Kaur, P., Kumar, S., Negi, N.S., Rao, S.M.: Enhanced magnetism in Cr-doped ZnO nanoparticles with nitrogen co-doping synthesized using sol–gel technique. *Appl. Nanosci.* **5**(3), 367–372 (2015)
- Kelsall, R.W., Hamley, I.W., Geoghegan, M.: *Nanoscale science and technology*. Wiley, Chichester (2006)
- Khan, S.A., Noreen, F., Kanwal, S., et al.: Green synthesis of ZnO and Cu-doped ZnO nanoparticles from leaf extracts of *abutilon indicum*, *clerodendrum infortunatum*, *clerodendrum inermis* and investigation of their biological and photocatalytic activities. *Mater. Sci. Eng.* **82**, 46–59 (2018a)
- Khan, R., Zulfikar, C.I., de Araujo, L., et al.: Influence of oxygen vacancies on the structural, dielectric, and magnetic properties of (Mn, Co) co-doped ZnO nanostructures. *J. Mater. Sci. Mater. Electron.* **29**(12), 9785–9795 (2018b). <https://doi.org/10.1007/s10854-018-9018-z>
- Khan, R., Zulfikar, de Araujo, C.I.L., et al.: Effect of thermal calcination on the structural, dielectric and magnetic properties of (ZnO–Ni) semiconductor. *J. Mater. Sci. Mater. Electron.* **30**(4), 3396–3404 (2019)
- Li, S., Song, H., Yu, H., et al.: Influence of annealing temperature on photoluminescence characteristics of Gd₂O₃:Eu/AAO nanowires. *J. Lumin.* **122**, 876 (2007)
- Li, C., Zang, Z., Han, C., et al.: Enhanced random lasing emission from highly compact CsPbBr₃ perovskite thin films decorated by ZnO nanoparticles. *Nano Energy* **40**, 195–202 (2017)
- Liu, Y., Yang, J., Guan, Q., et al.: Effects of Cr-doping on the optical and magnetic properties in ZnO nanoparticles prepared by sol–gel method. *J. Alloys Compd.* **486**, 835–838 (2009)
- Moazzen, M.A.M., Borghei, S.M., Taleshi, F.: Change in the morphology of ZnO nanoparticles upon the reactant concentration. *Appl. Nanosci.* **3**, 295–302 (2013)
- Murugan, R., Kashinath, L., Subash, R., et al.: Pure and alkaline metal ion (Mg, Ca, Sr, Ba) doped cerium oxide nanostructures for photo degradation of methylene blue. *Mater. Res. Bull.* **97**, 319–325 (2018)
- Omri, K., Najeh, I., El Mir, L.: Influence of annealing temperature on the microstructure and dielectric properties of ZnO nanoparticles. *Ceram. Int.* **42**, 8940–8948 (2016)
- Pushpalatha, C., Suresh, J., Gayathri, V.S., et al.: Zinc Oxide Nanoparticles: A Review on Its Applications in Dentistry. *Front. Bioeng. Biotechnol.* (2022). <https://doi.org/10.3389/fbioe.2022.917990>
- Reddy, A.J., Kokila, M.K., Nagabhushana, H., et al.: Structural, optical and EPR studies on ZnO: Cu nanopowders prepared via low temperature solution combustion synthesis. *J. Alloys Compd.* **509**, 5349–5355 (2011)
- Sadeq, M.S., Ibrahim, A.: The path towards wide-bandgap and UV-transparent lithium phosphate glasses doped with cobalt oxide for optical applications. *J. Non-Cryst. Solid* **569**, 120983 (2021)
- Sahal, M., Hartiti, B., Ridah, A., et al.: Structural, electrical and optical properties of ZnO thin films deposited by sol–gel method. *Microelectron. J.* **39**(12), 1425–1428 (2008)
- Salahuddin, N.A., El-Kemary, M., Ibrahim, E.M.: Synthesis and characterization of ZnO nanoparticles via precipitation method: effect of annealing temperature on particle size. *Nanosci. Nanotechnol* **5**(4), 82–88 (2015)
- Samkaria, R., Sharma, V.: Effect of rare earth yttrium substitution on the structural, dielectric and electrical properties of nanosized nickel aluminate. *Mater. Sci. Eng. B* **178**, 1410–1415 (2013)
- Sanad, M.M., Abdellatif, H.A., Elnaggar, E.M.: Understanding structural, optical, magnetic and electrical performances of Fe- or Co-substituted spinel LiMn_{1-x}Ni_xO₄ cathode materials. *Appl. Phys. A.* **125**, 1 (2019)

- Sangeetha, R., Muthukumar, S., Ashokkumar, M.: Structural, optical dielectric and antibacterial studies of Mn doped Zn_{0.96}Cu_{0.04}O nanoparticles. *Spectrochim. Acta. A. Mol. Biomol. Spectrosc.* **144**, 1–7 (2015)
- Saravanan, R., Santhia, K., Sivakumar, N., et al.: Synthesis and characterization of ZnO and Ni doped ZnO nanorods by thermal decomposition method for spintronic application. *Mater. Charact.* **67**, 10–16 (2012)
- Sayed, M.I., Ibrahim, A., Abdo, M.A., et al.: The combination of high optical transparency and radiation shielding effectiveness of zinc sodium borate glasses by tungsten oxide additions. *J. Alloys. Compd.* **904**, 164037 (2022)
- Shah, A.H., Zargar, R.A., Arora, M., et al.: Fabrication of pulsed laser-deposited Cr-doped zinc oxide thin films: structural, morphology, and optical studies. *J. Mater Sci: Mater Electron* **31**, 21193–21202 (2020)
- Shan, F.K., Yu, Y.S.: Band gap energy of pure and Al-doped ZnO thin films. *J. European. Ceramic. Soci* **24**, 1869–1872 (2004)
- Sharma, V.K., Najim, M., Srivastava, A.K., et al.: Structural and magnetic studies on transition metal (Mn, Co) doped ZnO nanoparticles. *J. Magn. Magn. Mater.* **324**, 683–689 (2012)
- Siddheswaran, R., Mangalaraja, R.V., Gomez, M.E., et al.: Room temperature ferromagnetism in combustion synthesized nano-crystalline Co, Al Co-doped ZnO. *J. Alloys. Compd* **581**, 146 (2013)
- Sirijan, T., Yongvanich, N.: Nanostructure of Cr-doped ZnO thin films by dip coating. *Mater. Res. Innov.* **18**, 174–178 (2014)
- Soitah, T.N., Chunhui, Y., Liang, S.: Effect of Fe Doping on Structural and Electrical Properties of Nanocrystalline ZnO Thin Films Prepared by Sol–Gel Dip Coating Technique. *Sci. Adv. Mater.* **2**(4), 534–538 (2010). <https://doi.org/10.1166/sam.2010.1120>
- Srinivasulu, T., Saritha, K., Ramakrishna, K.T.: Reddy, Synthesis and characterization of Fe-doped ZnO thin films deposited by chemical spray pyrolysis. *Mod. Electron. Mater* **3**(76), 85 (2017)
- Tabib, A., Sdiri, N., Elhouichet, H., et al.: Investigations on electrical conductivity and dielectric properties of Na doped ZnO synthesized from sol gel method. *J. Alloys Compd.* **622**, 687–694 (2015)
- Wang, X., Zheng, R., Liu, Z., et al.: Structural, optical and magnetic properties of Co-doped ZnO nanorods with hidden secondary phases. *J. Nanotechnol* **19**, 455702 (2008)
- Wang, M., Gao, Y., Dai, L., et al.: Influence of surfactants on the morphology of SnO₂ nanocrystals prepared via a hydrothermal method. *Solid State Chem.* **189**, 49–56 (2012)
- Wang, X.L., Luan, C.Y., Shao, Q., et al.: Effect of the magnetic order on the room-temperature band-gap of Mn-doped ZnO thin films. *Appl. Phys. Lett.* **102**, 102112 (2013)
- Wang, H., Cao, S., Zang, Z., et al.: NH₄Cl-modified ZnO for high-performance CsPbI₃ 2 perovskite solar cells via low-temperature process. *Solar Rrl.* **4**, 1900363 (2020)
- Wörner, C.H., Hazzledine, P.M.: Grain growth stagnation by inclusions or pores. *JOM* **44**, 16–20 (1992)
- Xiao, W., Zhang, J., Qin, M., et al.: ZnO electron transporting layer engineering realized over 20% efficiency and over 1.28 V open-circuit voltage in all-inorganic perovskite solar cells. *EcoMat* (2022). <https://doi.org/10.1002/eom2.12192>
- Zahabi, S., Jamali, H., Bakhshi, S.R., et al.: Comparing infrared transmission of zinc sulfide nanostructure ceramic produced via hot pressure and spark plasma sintering methods. *Int. J. Appl. Ceram. Technol.* **19**, 1319–1327 (2022)
- Zak, A.K., Razali, R., Majid, Abd, et al.: Synthesis and characterization of a narrow size distribution of zinc oxide nanoparticles. *Int. J. Nanomed.* **6**, 1399 (2011)
- Zargar, R.A., Ahmad, P.A., Gogre, M.A.S., Hassan, M.M.: Screen printing coating of (ZnO)_{0.8}(CdO)_{0.2} material for optoelectronic applications. *Opt. Quant. Electron.* **52**(9), 1–12 (2020)
- Zhao, Y., Zhou, W., Wang, Y., et al.: The Effect of humic acid and bovine serum albumin on the adsorption and stability of ZnO Nanoparticles on powdered activated carbon. *J. Clean. Prod.* **251**, 119695 (2020)